Journal of Thermal Science Vol.31, No.6 (2022) 1959–1969

https://doi.org/10.1007/s11630-022-1653-2 **Article ID: 1003-2169(2022)06-1959-11**

Study on Thermal Characteristics of a Novel Glass Curtain Wall System

FENG Chaoqing[1], CHEN Xin'ge[1], WANG Rui[2*], XU Zhao[1], ZHANG Lizhuang[1], YAN Suying[1]

1. College of Energy and Power Engineering, Inner Mongolia University of Technology, Hohhot 010051, China
2. China National Institute of Standardization, Beijing 100191, China

Abstract: In order to solve the conflict between indoor lighting and PV cells in building-integrated photovoltaic/thermal (BIPV/T) systems, a glass curtain wall system based on a tiny transmissive concentrator is proposed. This glass curtain wall has a direct influence on the heat transfer between indoor and outdoor, and the operating parameters of air and water inlet temperature, indoor and outdoor temperature, and radiation intensity have a significant influence on the heat transfer characteristics of the glass curtain wall. The 3D model is established by SoildWorks software, and the thermal characteristics of the new glass curtain wall system are simulated through computational fluid dynamics (CFD) method. Thermal performance was tested under actual weather for the winter working conditions. The CFD simulation results are verified by the test results under actual weather. The results show that thermal efficiency simulation results are in good agreement with the experimental results of the new glass curtain wall system. The simulation conditions were designed by using the orthogonal method, and the significance analysis of the influencing factors of the indoor wall surface heat gain was carried out. With the increase of the bottom heat flux and the air velocity, the heat absorption of the inner wall surface increases. When the wind speed is 0.1 m/s, the heat flow on the bottom surface rises from 500 W/m^2 to 2500 W/m^2, and the heat flow intensity on the interior wall changes from 10.31 W/m^2 to –29.12 W/m^2. Under typical working conditions, the new glass curtain wall system can reduce the indoor heat load by 47.5% than ordinary glass curtain wall.

Keywords: glass curtain wall, thermal characteristics, orthogonal experimental design, significant influencing factors

1. Introduction

Solar energy has become a hot spot in clean energy research with its inexhaustible and huge advantages [1]. Building energy consumption has accounted for one third of the total social energy consumption, so reducing building energy consumption is also one of the main goals of solar green building. The glass curtain wall in the building is the main source of indoor heat load, so people started to use solar energy on the glass curtain wall at the earliest. Photovoltaic power generation technology was started in 1954 at Bell Labs in the United States [2]. And in 1978, Kern et al. [3] proposed the concept of PV/T. According to PV/T, people proposed building-integrated photovoltaic/thermal (BIPV/T) systems in the early 1990s [4]. The system can make full

Special column: Built Thermal Environment GE: ZHAO Xudong
Received: Apr 27, 2021 AE: LIU Qibin
Corresponding author: WANG Rui E-mail: wangrui@cnis.ac.cn

Nomenclature

Symbols

c	air specific heat capacity/kJ·(kg·°C)$^{-1}$	T_1	inlet air temperature/°C
E_0	normal irradiance/W·m^{-2}	T_2	outlet air temperature/°C
K_i	the sum of the indoor wall surface heat flux corresponding to the horizontal number i under this factor	v	fan outlet wind speed/m·s^{-1}
L	number of level	W_{indoor}	heat for interior surface/W
n	number of working conditions	W_s	instantaneous solar energy/W
Q	heat gain/W	**Greek symbols**	
q_{in}	heat flux for interior surface/W·m^{-2}	η	thermal efficiency/%
S	cover surface area/m^2	ρ	air density/kg·m^{-3}
SS	variance	**Abbreviations**	
s	outlet area/m^2	CFD	Computational Fluid Dynamics
s_{in}	surface area for interior surface/m^2	CPC	Compound Parabolic Concentrator
T	sum of heat flux under all conditions	PMMA	Polymethyl methacrylate

use of building external surface to further reduce the cost of building materials, installation and maintenance, and use the flow of fluid to reduce the temperature of solar cells, improve the power generation efficiency, and prolong the service life of cells [5, 6]. Fu et al. [7] compares solar thermal system, photovoltaic system and PV/T system in the experiment, and finds that PV/T system is the best energy saving device in building energy consumption. Baklouti I. et al. [8] designed a PVT-air solar system, and found that increasing the airflow rate can improve the thermal efficiency through the experimentation and simulation, but the power output changes a little. However, the reduction in depth shows an increase in thermal efficiency, while the impact on electrical efficiency is negligible. Shen et al. [9] proposed a kind of cooling pipes embedded in the venetian blinds of a double-skin envelope as a system to reduce the heat transfer of the glass envelope in summer. The experiment shows that it effectively improved the indoor thermal comfort in summer. Yadav S. et al. [10] investigated the performance of an optimally tilted semi-transparent BIPV/T system influenced by shadow effect of four neighboring buildings. Panda SK et al. [11] evaluated the thermal performance of the semi-transparent BIPV panel with the best tilt angle. And Ting et al. [12] studied the multi-inlet system. The results show that the thermal efficiency of the multi-inlet system is 7% higher than that of the single-inlet system. A large number of simulations and experiments on BIPV/T in the above literature show that the system efficiency can be improved by optimizing the system structure, adjusting the angle and increasing the fluid contact area.

However, indoor lighting needs to be considered. In order to absorb more energy, it is necessary to increase the area of solar cells, but this will affect the indoor lighting. Therefore, it is particularly important to solve the conflict between lighting and power generation in BIPV.

With advances in electrochromic glass technology, many studies have used this method to control the sunlight entering a room, thereby regulating the heat load. Myunghwan O. et al. [13] developed an electrochromic glass with variable sunlight control and high solar radiation inhibition ratio and analyzed its influence on load reduction. Compared with the old curtain wall office building, four kinds of Polymer Dispersed Liquid Crystal (PDLC) films respectively energy saving 17.0%, 15.8%, 7.3% and 3.1%. M. Arnesano et al. [14] proposed a complete design method of thermochromic glass based on building energy consumption simulation, and the results showed that in some areas, its energy consumption and other aspects were better than standard transparent glass. Liang et al. [15] designed a translucent perovskite solar cell (ST-PSC) for smart Windows. The solar cell and glass curtain wall are integrated in design, and both color and transparency can be adjusted. Compared to traditional opaque solar cells, ST-PSC has unique applications with color adjustability, high transparency and other features that go beyond power generation.

Li et al. [16] designed a double-circulation water window. The window is composed of four layers of glass and two layers of water. The solar energy is used to preheat domestic hot water and the indoor temperature is adjusted through the window, which contributes to building energy saving. In addition, system efficiency can be improved by concentrating. Li et al. [17] proposed Lens-walled CPC (Compound Parabolic Concentrator) structure, which does not require tracking at all, and solves the difficulty of combining the general

concentrating devices with buildings, complex tracking systems, large initial investment. At the same time, the concentrating device can effectively increase the heat output temperature of the system. Wei et al. [18] designed and developed a building façade integrated asymmetric compound parabolic photovoltaic (BFI-ACP-PV) concentrator with the concentrating ratio of 2.0. The experimental results showed that the developed BFI-ACP-PV system has a potential to increase the output power per unit solar cell area by a factor of 2. Meng et al. [19] proposed a PV/T/D system for skylights by combining solar collectors with CPC. The simulation and experimental results show that the thermal efficiency of the heat recovery system ranges from 40% to 85% according to different inlet velocity and system geometry. Huang et al. [20] conducted a comprehensive study on the thermal and power performance of a new type of vacuum photovoltaic insulated glass device (VPV IGU). The comparative analysis showed that the thermal insulation performance of VPV IGU was excellent. In Hong Kong and Harbin, the heat gain and heat loss can be reduced by 81.63%, 75.03% and 31.94%, 32.03% respectively. Feng et al. [21] proposed a PV/T/D system composed of solid CPC and used it to manufacture transparent roofs, which can realize light control and regulate the indoor thermal environment of buildings. The system takes lighting and energy supply into account, which effectively reduces building energy consumption. Zheng et al. [22] developed a bionic nanostructured translucent organic photovoltaic cell, which has great potential as a solar energy conversion source mounted on glass curtain walls. Hong et al. [23] proposed a new type of transmissive concentrating system for glass curtain wall; the experimental results show that the lowest transmittance of the system is 28.2% at noon, and the transmittance can exceed 55% before 09:40 and after 15:40. The glass curtain wall system based on the new transmission concentrating system can realize the light control function well.

In order to solve the problem of PV and indoor lighting competition, as well as the indoor overheating and dazzling caused by direct sunlight at noon, according to the low cost of CPC, the large receiving angle, and the condensing effect of direct light and the high level of oblique incident light by the transmissive CPC micro-condensing unit, a new type of glass curtain wall system was designed using the hollow CPC water-passing structure. Research has been carried out on the thermal characteristics of the device; the correctness of the simulation model is verified through experiments, and the significant factors affecting the heat flow on the inner wall are analyzed through CFD, which provides a basis for large-scale applications in the future.

2. Structure and Working Principle

The glass curtain wall system is composed of multiple hollow tiny light-concentrating units, and the devices are all made of Polymethyl Methacrylate (PMMA). As shown in Fig. 1, the width of the experimental device *a* is 295 mm, and the height *b* is 65 mm. The upper cover is composed of 20 hollow CPC; the concentration ratio of the hollow CPC is 3.14, which means the light entrance width *d* is 12.56 mm and the light receiving surface width *e* is 4 mm; the ratio between *d* and *e* is 3.14; the height *c* is 25 mm, and the hollow part is filled with cooling fluid-water; PV cells are attached to the bottom of CPC, and the air inlets and outlets are set on both sides of the side panels. The air flows between the CPC and the bottom glass, and the heat generated by the photovoltaic cells is taken away by the flow of water and air.

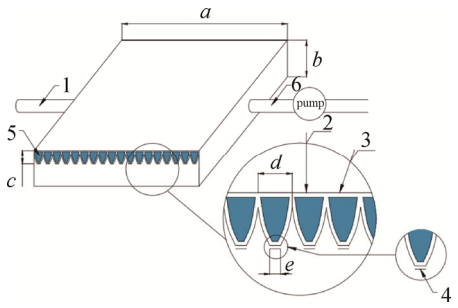

1. Air inlet, 2. Effective concentrating light, 3. Effective lighting, 4. Solar cell, 5. Cooling water, 6. Air vent

Fig. 1 Working principle of the new glass curtain wall

The structure is shown in Fig. 1, and the working principle is as follows: When sunlight enters the glass curtain wall system, there are two kinds of light: one is effective concentrating light 2, and the other is effective lighting 3. Through the concentrated action of CPC, the solar light is concentrated on the solar cell 4 at the bottom. After the receiving of light, the solar cell generates electricity and heat. The effective lighting 3 refracts and reflects inside the CPC, and finally shoots out at the lower side wall of the CPC. A vent is opened on both sides of the side panel, one air inlet and six air outlets, and a fan is added to the air outlet. By starting the fan, the air in the glass curtain wall system can flow, and the solar cells can be cooled by air and water at the same time. After being heated, the air and water can be used for heat source, realizing the combination of concentrated photovoltaic and solar heat, thereby improving the comprehensive utilization rate of energy.

The shape of concentrator has a significant effect on the optical properties. The authors have studied the curve form, wall thickness, height, concentration ratio and other factors of the concentrator in detail in Ref. [23]. Combined with the actual use of the glass curtain wall,

the suitable structural parameters are finally selected and used in this paper.

This kind of glass curtain wall system has the advantages of electricity generation, passive light control and high utilization rate of energy, and thus has practical value. When the incident angle of light is small, the reception rate of the system is high, and most of the light is received by the solar cells, which effectively alleviates the problem of dazzling and overheating problems caused by direct sunlight at noon. When the incident angle of light is larger, the transmission rate of the system is larger, which can effectively provide indoor lighting. Through the heat generated by the solar cell power generation, and the double cooling of air and water, the reduction of the temperature of the solar cells works, improving the work efficiency and service life of the solar cell. And the recovery of heat from the system can be carried out for secondary use, thereby effectively reducing the building energy consumption.

3. CFD Model Construction and Experimental Verification

As a part of the building palisade structure, the heat transfer characteristic of new glass curtain wall system affects the control strategy of each operating parameter in the use process. The indoor and outdoor ambient temperature, solar radiation, air velocity, water flow velocity and cooling water temperature affect the heat transfer of the system. In order to study the heat transfer characteristics of the system, CFD was used to simulate the new glass curtain wall system, and the simulation results were verified by experiments.

3.1 Establishment of numerical calculation model

According to the structure of the new glass curtain wall system, 20 tiny condensing units, each with a length of 600 mm, are selected to build a 3D simulation model, as shown in Fig. 2(a). The photovoltaic cells are attached to the tiny condensing units, and the photovoltaic cells are cooled simultaneously with the cooling medium of 1 and 3, so as to reduce the working temperature of the battery and to improve the working efficiency of the system.

3.2 Grid subdivision

ICEM CFD 19.2 software is used to divide the grid into tetrahedral grids. The number of grid nodes is 1 490 000, as shown in Fig. 2(b).

The model is divided into three parts: solar cells, hollow CPC and shell composed of solid named PMMA; air flow area is named air; the cooling water flow area is named water. The materials used in each zone and their thermophysical properties are listed in Table 1.

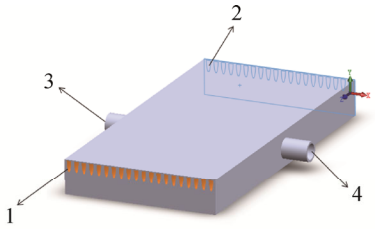

(a) 3D model

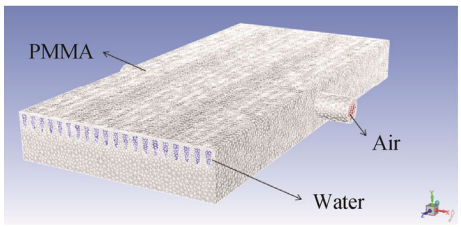

(b) Grid

1. Cooling water inlet, 2. Cooling water outlet, 3. Air inlet, 4. Air outlet

Fig. 2 The simulation model

Table 1 Material properties

Material	PMMA	Air	Water
Density/kg·m^{-3}	1200	1. 225	998. 2
Specific heat capacity /J·(kg·°C)$^{-1}$	1500	1006. 43	4182
Thermal conductivity /W·(m·°C)$^{-1}$	0. 2	0. 00242	0. 6

In addition, the verification of grid independence was carried out. Four sets of grids were designed from sparse to dense, and the number of grid nodes was 730 000, 1 490 000, 2 500 000 and 3 010 000, respectively. Under the working condition with the water temperature of 20°C and water speed of 0.001 m/s, the air temperature is 26°C; the air velocity is 0.1 m/s, and the heat flux intensity of the bottom surface is 2500 W/m^2. The results are shown in Fig. 3. It can be seen that: when the number of grids exceeds 1.5 million, the change of simulation results is very small as the number of grids increases, so the accuracy requirement of calculation results can be met when the number of grids is 1.5 million.

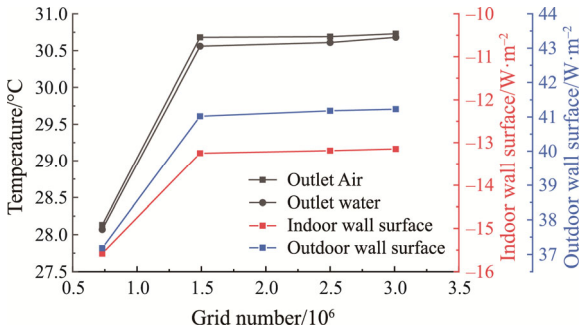

Fig. 3 Grid-independent result

3.3 Boundary condition setting and result analysis

According to the operation state of the new glass curtain wall during actual use, the CFD boundary conditions are determined as follows:

(1) Air inlet: inlet vent, and the measured value is brought into CFD according to the test, with the value of 3.5 m/s.

(2) Air outlet: pressure - outlet.

(3) Heat flux intensity of bottom: wall, numerical value is the irradiance at the time of the test multiplied by the concentration ratio of CPC.

(4) Hollow CPC and shell selected as solid, material for PMMA.

(5) Water inlet: inlet velocity.

(6) Water outlet: pressure outlet.

(7) The interface between solid and gas automatically defaults to the wall, and the boundary conditions are coupled.

Under the working condition with the water temperature of 20°C and water speed of 0.001 m/s, as an example, the air temperature is 26°C; the air speed is 0.1 m/s, and the heat flux intensity of the bottom surface is 2500 W/m^2. The results are shown in Figs. 4–6.

Fig. 4 shows the distribution of temperature field along the direction of air flow. The left side is the air inlet, and the right side is an air outlet; the yellow strip is the heat produced when the solar cell produces electricity. And the results show that the low temperature air absorbs the heat generated by solar cells, and the final air temperature increases from 26°C to 30.5°C. When the air inlet temperature is low, the cooling effect of the air flow near the inlet side is more obvious. With the air flowing in the air cooling region, the temperature difference

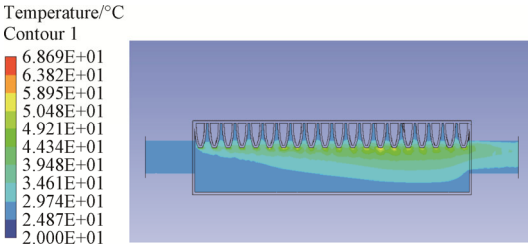

Fig. 4 Distribution of air temperature

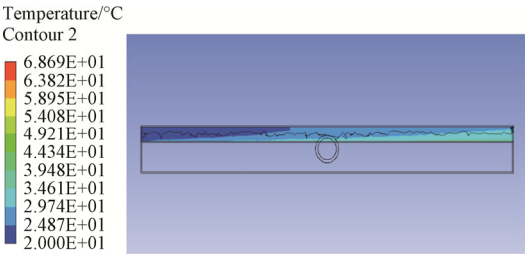

Fig. 5 Distribution of water temperature

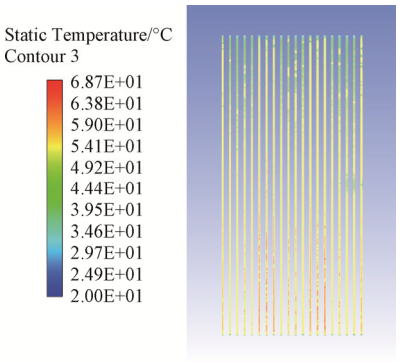

Fig. 6 Distribution of PV temperature

between the photovoltaic cell and the air becomes smaller, and the cooling effects gradually become weak. Fig. 5 is the calculation results of temperature distribution along the direction of water flow. The left side is the water inlet, and the right side is water outlet. Since the inlet temperature of the water stream is lower than that of the air, the cooling water not only absorbs heat generated by photovoltaic cells but also absorbs heat of air during the flow process. The average outlet temperature of water flow is about 30.5°C. It can be seen from the temperature distribution results of photovoltaic cells in Fig. 6 that the surface temperature of photovoltaic cells changes significantly along the water flow direction, while the temperature changes slightly along the air flow direction. The main reason is that the inlet temperature of water is lower, and the specific heat is larger; thus the water cooling effect is more obvious.

3.4 Test validation

In order to verify the accuracy of the simulation model, winter condition was selected to carry out the experiment. Test conditions are set as follows: The air inlet and outlet are connected to the ambient atmosphere; the water circulation inlet is connected with the constant temperature water bath. The experimental schematic diagram is shown in Fig. 7. After the light enters the system, the battery generates power and heat, and records solar irradiance, air outlet temperature and velocity, battery power at this time. The outlet air velocity is measured by TESTO-425 and the range is 0–20 m/s. The radiation intensity is measured by TRM-ZS2 irradiator, and its range is 0–2000 W/m^2. In order to reduce the indoor heat release to the environment, the hollow part of CPC is filled with water which does not flow during the experiment. The experimental bench is mainly composed of a new glass curtain wall cover plate, integral box, irradiation meter, fan, wind speed and temperature measuring instrument, and a photovoltaic cell is installed at the bottom of the CPC. The photovoltaic cell used in the test is a common flexible cell in the market as shown in Fig. 8. Its width is the same as that of the bottom of the

CPC, and the length of the removed electrode part is same as that of the whole CPC. In order to ensure the stability of wind speed during the test, the voltage is adjusted by transformer before the test, so that the outlet wind speed is stabled at 3.5 m/s.

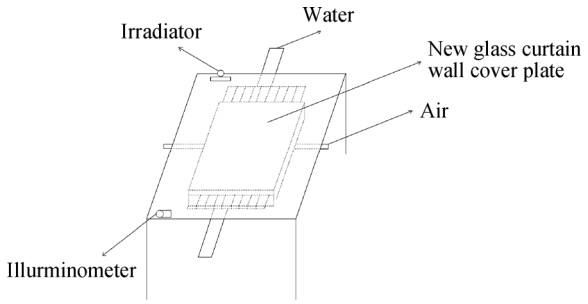

Fig. 7 Experimental principles

Fig. 8 Thermal performance test bench

3.4.1 Test method

The device is placed on the horizontal floor to ensure that one side of the device is perpendicular to the south direction, and the rear end of the unit is raised by using a foam block, to ensure that the sun incidence angle at true solar time is 0°, which is convenient for comparison with the simulation results. The total solar radiation value was recorded at E_0 (W/m^2), the inlet air temperature T_1 (°C) and the outlet air temperature T_2 (°C) every 15 minutes.

The instantaneous solar energy on the surface of the new glass curtain wall cover is:

$$W_s = E_0 \cdot S \tag{1}$$

where, E_0 is a normal irradiance, W/m^2; S is cover surface area, m^2; The heat gain is Q:

$$Q = c \cdot v \cdot p \cdot s \cdot \Delta t \tag{2}$$

where, c is air specific heat capacity, kJ/(kg·°C); v is fan outlet wind speed, m/s; ρ is air density, kg/m^3; s is outlet area, m^2; Δt is the difference between T_2 and T_1.

The thermal efficiency η of the new glass curtain wall system at this time is:

$$\eta = \frac{Q}{W_s} \tag{3}$$

3.4.2 Test results and analysis

According to the calculation, the maximum solar altitude angle at experiment location was about 29°, and it was 12:11 in true solar time. Under actual weather conditions, the experimental results of system thermal/electrical efficiency are shown in Fig. 8. After the test, the solar radiation intensity, inlet temperature and fan outlet velocity recorded in the test are introduced into CFD. Since the concentration ratio of CPC is 3.14, the irradiance at this time point needs to be multiplied by 3.14 in the numerical calculations. After the equation converges, the outlet temperature at this point is obtained, and then the simulated heat generation efficiency is obtained through the calculation formula.

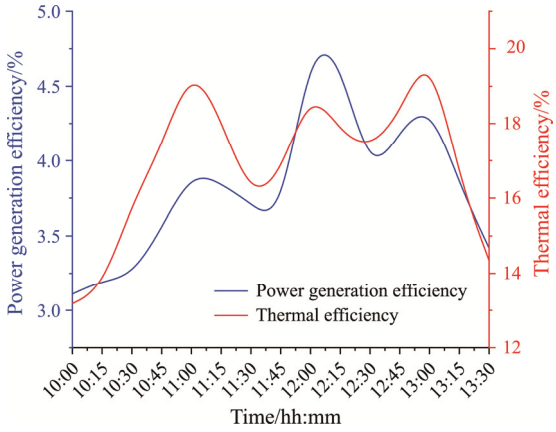

Fig. 9 Comparison curve of experimental electrical/thermal efficiency

It can be seen from Fig. 9 that the test time ranges from 10:00 to 13:30. As time goes on, the test electrical/thermal efficiency curve becomes wave-shaped. At 10:00, the thermal efficiency is 13.18%, and the electrical efficiency is 3.11%. And both of the values increase with time. At 11:00, the thermal efficiency is 19.66% and the electrical efficiency is 3.93%. From 11:00 to 12:00, the curve first drops and then rises. At 12:00, the electrical efficiency reaches the test maximum value of 4.81%, and the thermal efficiency is 19.01%. From 12:00 to 13:00, the curve first drops and then rises. At 13:00, the thermal efficiency reaches the test maximum value of 20.15%, and the electrical efficiency is 4.4%. After 13:00, both of the values gradually decrease with the passage of time.

The comparison of heat generation efficiency results of experimental test and simulation is shown in Fig. 10. Among them, for the simulation of the thermal characteristics, according to the operating conditions of the system under actual weathers, the boundary conditions in Fluent are set as follows:

(1) Air inlet: The air flow rate was at 0.002 m^3/s and

same as experiment. The inlet temperature is the ambient temperature under actual weathers.

(2) Air outlet: pressure - outlet.

(3) The liquid in the microchannel is full of and not flow in winter condition.

(4) Heat flux intensity of bottom is set based on the optical numerical results and value is the irradiance at the time of the test multiplied by the concentration ratio of CPC.

(5) Outer wall: The outdoor wall temperature is consistent with the ambient temperature.

(6) Inner wall: The indoor wall temperature is set with temperature inside the box.

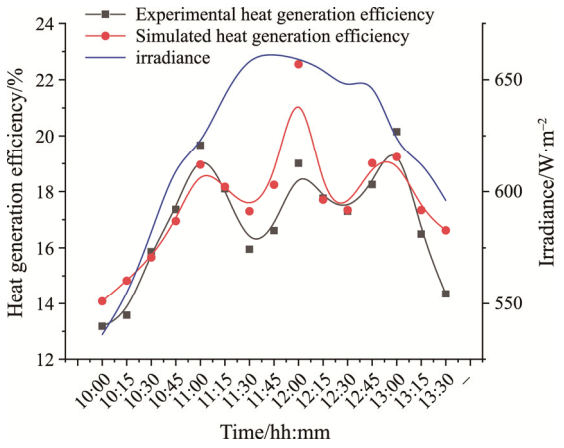

Fig. 10 Comparison curve of experimental heat generation efficiency and simulated heat generation efficiency

It can be seen from Fig. 10 that the test thermal efficiency is basically the same as the simulation thermal efficiency, which verifies the correctness of the numerical calculation model well. The thermal efficiency of system is higher when the sunlight is direct or the incident angle is small. For example, in the time range of 11:00 to 13:00, the maximum thermal efficiency of system reaches 20% at 13:00. When the incident angle is large, the heat generation of the system is low. For example, the heat generation efficiency is 13% at 10:00. However, the comparison between the experimental results and the simulation results shows that although the trend is basically the same, the specific values are quite different. The reason is that the test is carried out outdoors, the ambient temperature is low, and the heat loss is large. Through experiments, it is found that the new glass curtain wall system has the highest reception rate at noon (11: 00–13: 00), reaching 80%. At this time, the direct sunlight is concentrated on the solar cells by the hollow CPC to generate electricity and heat, and the photoelectric conversion efficiency reaches the peak; the maximum thermal efficiency is 19%, and the electrical efficiency is 4.6%. The system can alleviate the problems of indoor overheating and dazzling caused by direct sunlight at noon, and at the same time, it can use the excess light to generate heat and electricity, which effectively improve the comprehensive energy utilization rate of the system, and reduce building energy consumption.

4. Thermal Characteristic Simulation

The reliability of the CFD calculation model is verified through experimental tests. In order to further study the thermal characteristics of system, there are five main factors affecting the thermal characteristics of the system: Air inlet temperature, air inlet velocity, cooling water inlet temperature, cooling water inlet velocity and solar irradiance. Therefore, the value range of each factor in the numerical calculation is relatively large, so the orthogonal method is adopted. Each factor is divided into five levels, and numerical simulation is used to study the influence of different factors on the thermal characteristics of system.

4.1 Determination of factor rank

In summer, the air inlet temperature of the simulation system is maintained at 26°C to 34°C, and the water inlet temperature maintained at 20°C to 28°C. According to the previous literature investigation and single CPC working condition simulation, the water inlet velocity is set at 0.001 m/s to 0.02 m/s, and the air inlet velocity is set at 0.1 m/s to 2 m/s. And the CPC concentration ratio is 3.14 in optical simulation. When the sun enters the system vertically, the maximum energy flux density of the bottom solar cell is 2153 W/m^2, so the bottom heat flux range is set at 500 W/m^2 to 2500 W/m^2, and the factor level is shown in Table 2.

4.2 Analysis of orthogonal operating conditions

The five factors affecting the thermal characteristics of system are independent of each other, so the interaction is not considered in the process of orthogonal design. The working conditions and numerical results based on the orthogonal method are shown in Table 3, in which the empty column is also called the error column in the variance analysis of orthogonal design [24], and its role is to reduce the error.

Analysis of variance can be used to eliminate the influence of position magnitude and experimental error. The method is as follows [25]:

$$T = K_1 + K_2 + K_3 + K_4 + K_5 \tag{4}$$

$$P = \frac{T^2}{n} \tag{5}$$

Table 2 Factor rank

Level	Air temperature/°C	Air velocity/m·s^{-1}	Water temperature/°C	Water velocity/m·s^{-1}	Bottom heat flux/W·m^{-2}
1	26	0.1	20	0.001	500
2	28	0.5	22	0.005	1000
3	30	1	24	0.01	1500
4	32	1.5	26	0.015	2000
5	34	2	28	0.02	2500

Table 3 Conditions and results of orthogonal experiment

Number	Air temperature/°C	Air velocity /m·s^{-1}	Water temperature/°C	Water velocity/m·s^{-1}	Bottom heat flux/W·m^{-2}	Empty column	Indoor wall surface heat flux/W·m^{-2}
1	1	1	1	1	1	1	–0. 45
2	1	2	2	2	2	2	–4. 22
3	1	3	3	3	3	3	–13. 08
4	1	4	4	4	4	4	–26. 18
5	1	5	5	5	5	5	–41. 81
6	2	1	2	3	4	5	–8. 80
7	2	2	3	4	5	1	–18. 23
……				……			
19	4	4	2	5	3	1	–18. 17
20	4	5	3	1	4	2	–47. 80
21	5	1	5	4	3	2	–13. 19
22	5	2	1	5	4	3	–13. 45
23	5	3	2	1	5	4	–43. 87
24	5	4	3	2	1	5	–13. 53
25	5	5	4	3	2	1	–27. 73
K_1	–85. 75	–42. 99	–58. 81	–135. 87	–34. 33	–94. 92	
K_2	–70. 67	–66. 43	–77. 88	–76. 04	–67. 41	–98. 07	
K_3	–84. 47	–101. 20	–98. 16	–85. 26	–77. 66	–67. 81	
K_4	–97. 74	–106. 77	–96. 65	–66. 97	–126. 58	–98. 60	
K_5	–111. 80	–133. 04	–118. 94	–86. 29	–144. 45	–91. 03	

Note: K_i is the sum of the indoor wall surface heat flux corresponding to the horizontal number i (i=1, 2, 3, 4, 5) under this factor; k_i is the average value of K_i

Table 4 Variance table of indoor wall

	Air temperature /°C	Air velocity /m·s^{-1}	Water temperature /°C	Water velocity /m·s^{-1}	Bottom heat flux /W·m^{-2}	Empty column
K_1^2	7353. 33	1848. 14	3459. 20	18459. 91	1178. 82	9010. 06
K_2^2	4994. 49	4413. 04	6064. 83	5781. 75	4544. 38	9618. 24
K_3^2	7135. 72	10 240. 82	9634. 54	7270. 09	6031. 74	4598. 36
K_4^2	9553. 05	11 400. 36	9341. 22	4485. 08	16 021. 25	9721. 48
K_5^2	12 499. 00	17 700. 81	14 146. 12	7446. 74	20 865. 73	8286. 79
SS	191. 45	1004. 96	413. 51	573. 04	1612. 71	131. 31

$$Q = \frac{K_1^2 + K_2^2 + K_3^2 + K_4^2 + K_5^2}{L} \tag{6}$$

$$SS = Q - P \tag{7}$$

where, T is the sum of heat flux under all conditions; n is the number of working conditions; L is the number of level.

The variance analysis results of the indoor wall surface after calculation are shown in Table 4. The variance of air temperature is 191.44; the variance of air

Table 5 Significance test table of indoor wall

Project	Sum of squares	Degree of freedom	Mean square	F	F_a
Air temperature	191. 45	4	47. 86	1. 46	F0. 05(4. 4)=6. 388
Air velocity	1004. 96	4	251. 24	7. 65	
Water temperature	413. 51	4	103. 38	3. 15	
Water velocity	573. 04	4	143. 26	4. 36	
Bottom heat flux	1612. 71	4	403. 18	12. 28	
Error	131. 31	4	32. 83		

velocity is 1004.96; the variance of water temperature is 413.51; the variance of water velocity is 573.04, and the variance of bottom heat flux is 1612.71.

The data were substituted into the significance test table, as shown in Table 5. The sum of squares in the table is the variance *SS*, and the degree of freedom is the level minus 1. The mean square is obtained by the sum of squares dividing the degree of freedom. The F is obtained the mean square dividing the mean square of error. The F_a can be obtained by looking up the table. When the F of the factor is greater than F_a, it shows that the factor has a significant effect on the heat loss of indoor wall surface. Only when $F_{\text{heat flux}}$, $F_{\text{air velocity}} > F_a$, the bottom heat flux and air velocity have significant influence on the heat loss of indoor wall surface.

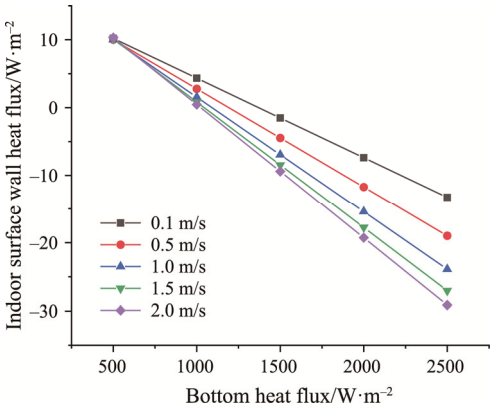

Fig. 11 Air speed-the influence curve of bottom heat flux on interior surface heat flux

4.3 Heat rule of interior surface

For the glass curtain wall system, the influence on the indoor heat load is the main issue to be considered in our design. Therefore, it is necessary to focus on the analysis of the influence of the system operating parameters on the indoor wall heat transfer law of the glass curtain wall.

In the previous section, the orthogonal design is adopted. Through the analysis of orthogonal results, it is concluded that the heat loss on the interior surface is mainly affected by the bottom heat flux and the air inlet velocity. In order to explore the influence of the above two conditions on the interior surface, the other three variables are set as quantitative (air inlet temperature 26°C, water inlet temperature 20°C, water inlet velocity 0.001 m/s). The indoor wall surface simulates the indoor temperature, and the temperature is constant at 26°C. The formula for calculating interior surface heat is as follows:

$$W_{\text{indoor}} = q_{\text{in}} \times s_{\text{in}} \tag{8}$$

where, W_{indoor} is heat for interior surface, W; q_{in} is heat flux for interior surface, W/m^2; s_{in} is surface area for interior surface, m^2.

The simulation results are shown in Fig. 11. It can be seen from the calculation results that with the increase of the bottom heat flux, the interior surface heat absorption gradually increases. When the velocity is 0.1 m/s, the bottom heat flux rises from 500 W/m^2 to 2500 W/m^2, and the wall heat flux changes from 10.31 W/m^2 to –13.25 W/m^2. When other variables are constant, the heat absorption of the interior surface increases with the increase of the velocity. Taking the bottom heat flux of 2500 W/m^2 as an example, when the velocity increases from 0.1 m/s to 2 m/s, the interior surface heat flux changes from 10.31 W/m^2 to –29.12 W/m^2.

4.4 Analysis of influence on indoor heat load

Taking the glass curtain wall of unit area as the research object, assuming that the midday solar irradiation is 1000 W/m^2, the shading coefficient of ordinary glass curtain wall is about 0.2, and about 800 W/m^2 heat enters the room through the glass curtain wall. According to the optical experiment test, the transmittance of the new glass curtain wall is about 34% at noon [23], and 340 W/m^2 heat enters the room through the new glass curtain wall. The analysis of thermal characteristics shows that under typical working conditions (outdoor temperature is 34°C; indoor temperature is 26°C; Water inlet temperature is 26°C, water inlet velocity is 0.001 m/s; Air inlet velocity is 0.1 m/s) The heat flow on the indoor side wall of the glass curtain wall is about 80 W/m^2, so the total heat transmitted into the interior through the new glass curtain wall is 420 W/m^2. Compared with the two glass curtain walls, the new glass curtain wall system can reduce the indoor heat load by 47.5%.

5. Conclusions

In this paper, the thermal characteristics of a new type of glass curtain wall system are studied. The conclusions are as follows:

(1) The thermal efficiency of the new glass curtain wall system calculated by the CFD simulation model is in good agreement with the experimental results, which indicates that the established simulation model can accurately calculate the heat transfer of the system.

(2) Based on the numerical calculation of the orthogonal working condition carried out by the simulation model, the significance analysis of the influencing factors of the indoor wall surface heat gain is carried out. The results show that the bottom heat flow and air velocity have significant influences on the heat loss of the indoor wall surfaces.

(3) With the increase of the heat flow at the bottom, the heat absorption of the interior surface gradually increases. When the wind speed is 0.1 m/s, the heat flow on the bottom surface rises from 500 W/m^2 to 2500 W/m^2, and the heat flow intensity on the interior wall changes from 10.31 W/m^2 to –29.12 W/m^2. Under typical working conditions, the new glass curtain wall system can reduce the indoor heat load by 47.5% than ordinary glass curtain wall.

Acknowledgements

This research was supported by the National Natural Science Foundation of China (51766013, 51766012), the Inner Mongolia Natural Science Foundation of China (2020LH05014, 2019MS05025), the Inner Mongolia Science and Technology Major Project in 2019.

References

[1] Wang G., Xu S., Han L., et al., Review on the major techniques and applications of photo-thermal utilization of solar energy. Materials Review, 2014, 28(S1): 193–196.

[2] Zhang S., Guan X., Wang D., et al., Research development of solar thermal utilization and photovoltaic power generation. Chemical Industry and Engineering Progress, 2012, 31(S1): 323–327.

[3] Kern Jr E.C., Russell M.C., Combined photovoltaic and thermal hybrid collector system. In: Proceedings of the13th IEEE photovoltaic specialists. Washington DC, USA, 1978, pp.1153–1157.

[4] Yang T., Athienitis A.K., A review of research and developments of building-integrated photovoltaic/thermal (BIPV/T) systems. Renewable and Sustainable Energy Reviews, 2016, 66: 886–912.

[5] Daniel C., Manuel I., Linear Fresnel concentrators for building integrated applications. Energy Conversion and Management, 2010, 51: 1476–1480.

[6] Ankita Gaur., G.N.Tiwari., Christophe M., et al., Numerical and experimental studies on a Building integrated Semi-transparent Photovoltaic Thermal (BiSPVT) system: Model validation with a prototype test setup. Energy Conversion and Management, 2016, 129: 329–343.

[7] Fu H., Zhao X., Ma L., et al., A comparative study on three types of solar utilization technologies for buildings: Photovoltaic, solar thermal and hybrid photovoltaic/ thermal systems. Energy Conversion and Management, 2017, 140: 1–13.

[8] Baklouti I., Driss Z., Numerical and experimental study of the impact of key parameters on a PVT air collector: mass flow rate and duct depth. Journal of Thermal Science, 2021, 30: 1625–1642.

[9] Shen C., Li X., Solar heat gain reduction of double glazing window with cooling pipes embedded in venetian blinds by utilizing natural cooling. Energy and Buildings, 2016, 112: 173–183.

[10] Yadav S., Panda S.K., Hachemvermette C., et al., Optimum azimuth and inclination angle of BIPV panel owing to different factors influencing the shadow of adjacent building. Renewable Energy, 2020, 162: 381–396.

[11] Yadav S., Panda S.K., Thermal performance of BIPV system by considering periodic nature of insolation and optimum tilt-angle of PV panel. Renewable Energy, 2020, 150: 136–146.

[12] Yang T., Andreas K., Athienitis, Performance evaluation of air-based building integrated photovolta-ic/thermal (BIPV/T) system with multiple inlets in a cold climate. Procedia Engineering, 2015, 121: 2060–2067.

[13] Myunghwan O., Sungho T., Sangkun H., Analysis of heating and cooling loads of electrochromic glazing in high-rise residential buildings in South Korea. Sustainability, 2018, 10(4): 1121.

[14] Arnesano M., Pandarese G., Martarelli M., et al., Optimization of the thermochromic glazing design for curtain wall buildings based on experimental measurements and dynamic simulation. Solar Energy, 2021, 216: 14–25.

[15] Shen L., Yip H., Gao F., Ding L., Semitransparent perovskite solar cells for smart windows. Science Bulletin, 2020, 65(12): 980–982.

[16] Li C., Li C., Lyu Y., et al., Performance of double-circulation water-flow window system as solar collector and indoor heating terminal. Building Simulation, 2020, 13(3): 575–584.

[17] Li G., Design and development of a Lens-walled compound parabolic concentrator-A review. Journal of Thermal Science, 2018, 28(1): 19–31.

[18] Wei L., Wu Y., Philip E., Design and development of a Building Façade Integrated Asymmetric Compound Parabolic Photovoltaic concentrator (BFI-ACP-PV). Applied Energy, 2018, 220: 325–336.

[19] Meng T., Xu Y., Su Y., et al., A study on incorporation of transpired solar collector in a novel multifunctional PV/Thermal/Daylighting (PV/T/D) panel. Solar Energy, 2018, 165: 90–99.

[20] Huang J., Xi C., Yang H., et al., Numerical investigation of a novel vacuum photovoltaic curtain wall and integrated optimization of photovoltaic envelope systems. Applied Energy, 2018, 229: 1048–1060.

[21] Feng C., Zheng H., Wang R., et al., A novel solar multifunctional PV/T/D system for green building roofs. Energy Conversion and Management, 2015, 93: 63–71.

[22] Zheng J., Sun Q., Gao C., et al., Toward ultra-low reflectance semi-transparent organic photovoltaic cells with biomimetic nanostructured transparent electrode. Organic Electronics, 2018, 60(9): 38–44.

[23] Hong M., Feng C., Xu Z., et al., Performance study of a new type of transmissive concentrating system for solar photovoltaic glass curtain wall. Energy Conversion and Management, 2019, 201: 112167.

[24] Panli, The thermal comfort investigation of awakening and sleeping state based on physiological parameters. Shanghai Jiaotong University, Shanghai, China, 2012.

[25] Wang W., Test design and analysis. First ed, Higher Education Press, Beijing, 2004.